Article ID: 1000-7032(2024)07-1156-07

AlGaN-based Deep Ultraviolet Light-emitting Diodes on Separated Multiple Quantum Barrier Electron Blocking Layer

SHEN Guowen[1,2], LU Lin[1,2*], XU Fujun[3], LYU Chen[1,2],
GAO Wengen[1,2], DAI Guangzhen[1,2]
(1. *Key Laboratory of Advanced Perception and Intelligent Control of High-end Equipment, Ministry of Education, Anhui Polytechnic University, Wuhu* 241000, *China*;
2. *School of Electrical Engineering, Anhui Polytechnic University, Wuhu* 241000, *China*;
3. *Research Center for Wide Gap Semiconductor, School of Physics, Peking University, Beijing* 100871, *China*)
* *Corresponding Author, E-mail: LLu-wh@qq.com*

Abstract: Separated multiple quantum barrier electron blocking layer (EBL) have been investigated to improve the performance of AlGaN-based deep ultraviolet light-emitting diodes (DUV-LEDs) with the wavelength shorter than 250 nm. It is confirmed that the DUV-LEDs with separated multi-quantum barriers EBL contribute to a much higher hole concentration and radiative recombination rate than the conventional block EBL configuration. Due to the formation of a hole acceleration zone by the separation interlayer in the EBL, the hole injection efficiency is significantly increased. Meanwhile, the multi-quantum barrier sample suppresses the electron leakage through raised electron barrier, thus significantly improves the device performance.

Key words: AlGaN; deep ultraviolet light-emitting diodes; electron blocking layer
CLC number: TN304.23　　**Document code**: A　　**DOI**: 10.37188/CJL.20240045

基于分离多量子垒电子阻挡层的AlGaN基深紫外发光二极管

申国文[1,2]，鲁　麟[1,2*]，许福军[3]，吕　琛[1,2]，高文根[1,2]，代广珍[1,2]
(1. 安徽工程大学 高端装备先进感知与智能控制教育部重点实验室，安徽 芜湖　241000；
2. 安徽工程大学 电气工程学院，安徽 芜湖　241000；
3. 北京大学物理学院 宽禁带半导体研究中心，北京　100871)

摘要：通过分离多量子垒电子阻挡层(EBL)结构，实现了AlGaN基DUV-LED器件性能的提升。由仿真结果可得，与传统的块状EBL相比，采用分离多量子垒结构的EBL可以获得更高的空穴浓度和辐射复合速率。这得益于EBL中间的夹层形成了空穴加速区，使得空穴在加速区获得能量，从而提高了空穴注入效率。另外，多量子势垒结构还能够通过提高电子势垒有效抑制电子泄漏，从而大幅度提升器件性能。综上所述，多量子垒电子阻挡层的引入可以显著提升AlGaN基DUV-LED器件的性能。

关　键　词：AlGaN；深紫外发光二极管；电子阻挡层

收稿日期：2024-02-24；**修订日期**：2024-03-25
基金项目：国家自然科学基金(61306108)；教育部留学回国人员科研启动基金(2013693)；安徽工程大学拔尖人才计划(20190508)
Supported by National Natural Science Foundation of China (61306108); Project-sponsored by SRF for ROCS, SEM (2013693); Program for the TOP talents of Anhui Polytechnic University (20190508)

1 Introduction

In recent years, AlGaN-based deep ultraviolet light-emitting diodes (DUV-LEDs) with short wavelengths[1] (<260 nm) have received increasing attention[2], due to their significant advantages of high efficiency, environment friendly[3], and portability and tunable wavelength[4]. Besides, from the perspective of environmental protection functions, shorter wavelength DUV-LEDs can effectively expand the application of ultraviolet light in the detection of toxic and harmful gases such as SO_2, NO, NH_3, *etc*[5], especially in the detection of NO and heavy metals such as Pb, Ni, Cd in soil, which have important application value[6]. Therefore, short wavelength DUV-LEDs have important application value and urgent demand in fields of public health, environmental protection, healthcare, and biochemical analysis.

In order to achieve high-performance short wavelength DUV-LED devices, it is crucial to inject a sufficient number of holes into the active region and effectively suppress electron leakage. However, as the emission wavelength of DUV-LEDs becomes shorter, the required Al composition of AlGaN will increase, making p-type doping more difficult, resulting in serious unbalance between n-type and p-type carriers and conductivity[7]. Lower hole concentrations and mobility will hinder hole injection into the quantum well region. Therefore, it has become crucial to improve the efficiency of hole injection while reducing electronic leakage[8]. To address the aforementioned issues, a series of solutions have been proposed, such as utilizing polarization effect to promote carrier injection[9], improving hole tunneling effect by introducing superlattice electron blocking layer (EBL) sample[10], and using polarization modulated electron blocking layer to prevent electron leakage[11]. Alternatively, hole injection can be improved by using the last layer of quantum barrier with an un-doped sample[12] or non-uniform doped sample[13]. In addition, some ideas for device samples in the broader wavelength range can also be adopted, such as polarization modulation at last quantum barrier[14] and a step-graded n-type AlInGaN EBL[15]. However, with effective suppression of electron leakage, the potential barrier for hole injection always increases. Therefore, seeking novel samples that can balance electron and hole injection is of special importance.

In this study, a separated multi quantum barrier EBL sample is proposed to achieve high-performance short wavelength DUV-LEDs. This sample can reduce the effective barrier for holes, significantly improve the hole injection efficiency in the active region and reduce the impact of electron leakage, thus effectively improving the performance and efficiency of DUV-LEDs with shorter wavelength.

2 Structure and Parameters

The DUV-LEDs with emission wavelength of 250 nm in this study is schematically shown in Fig. 1. sample A is designed to grow on a *c*-plane sapphire substrate with a 1-μm-thick AlN buffer layer and a 2-μm-thick Si-doped n-$Al_{0.71}Ga_{0.29}N$ with a n-type carrier concentration of 2×10^{18} cm^{-3} layer. The active area is made up of four pairs of 10-nm-thick $Al_{0.71}Ga_{0.29}N$ quantum barriers with a n-type carrier concentration of 1×10^{18} cm^{-3} and the additional quantum barrier of undoped 20-nm-thick $Al_{0.71}Ga_{0.29}N$ (no doped), whereas the quantum well is made up of four pairs of 1-nm-thick $Al_{0.49}Ga_{0.51}N$. Then, a 45 nm-thick Mg-doped p-type $Al_{0.8}Ga_{0.2}N$ EBL with a p-type carrier concentration of 1×10^{18} cm^{-3} followed by a 50-nm-thick p-type $Al_{0.72}Ga_{0.28}N$ with a p-type carrier concentration of 1×10^{18} cm^{-3}. Finally, as the contact layer, a 10-nm-thick p-type GaN layer with a p-type carrier concentration of 1×10^{18} cm^{-3} is adopted.

In comparison to the conventional sample A, samples B−C primarily differ in the design of the EBL. The EBL of sample B consists of three layers: 9-nm-thick $Al_{0.8}Ga_{0.2}N$, 28-nm-thick $Al_{0.7}Ga_{0.3}N$, and 8-nm-thick $Al_{0.8}Ga_{0.2}N$ in order. The EBL in sample C consists of 7 layers, comprising 4-nm-thick $Al_{0.8}Ga_{0.2}N$, 3-nm-thick $Al_{0.72}Ga_{0.28}N$, 2-nm-thick $Al_{0.8}Ga_{0.2}N$, 28-nm-thick $Al_{0.7}Ga_{0.3}N$, 2-nm-thick $Al_{0.8}Ga_{0.2}N$, 3-nm-thick $Al_{0.72}Ga_{0.28}N$, and 3-nm-thick $Al_{0.8}Ga_{0.2}N$. All EBL layers in both samples B and C are Mg-doped at a concentration of 1×10^{18} cm^{-3}.

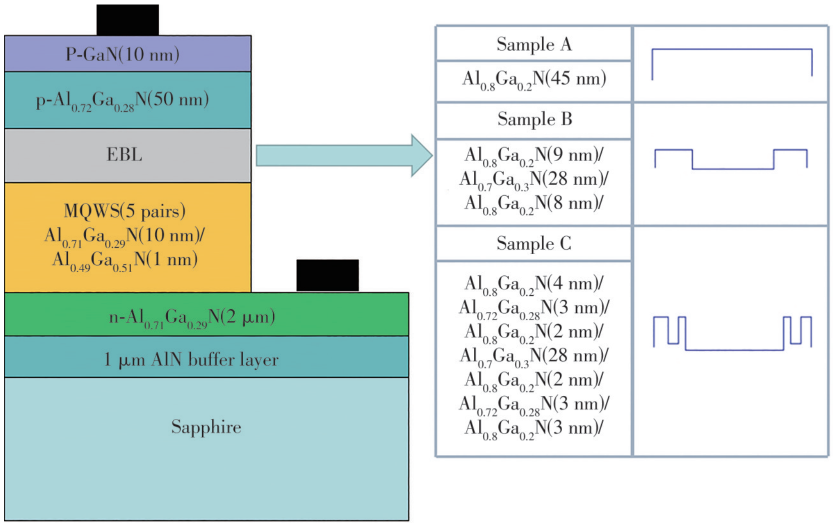

Fig.1 Schematic diagrams of samples A−C

In our numerical simulations, we employed the APSYS software to solve the self-consistent Poisson equation, continuity equation, and Schrödinger equation with appropriate boundary conditions[16]. The operating temperature was chosen as 300 K, and a Shockley-Read-Hall lifetime of 5 ns per quantum well was assumed, with an internal loss of 2 000 m^{-1}. The polarization effects were accounted for by incorporating polarization interface charges at each heterojunction[17].

Taking crystal relaxation induced by threading dislocations into consideration, we assumed a polarization level of 40% in our calculations. The Auger recombination coefficient was taken as 1.0×10^{-30} $cm^6\cdot s^{-1}$, which is similar to reported values[18]. The energy band offsets of the AlGaN-based DUV-LED were assumed to be $\Delta E_c/\Delta E_g$ = 0.7/0.3[19]. The bandgap of AlGaN is represented as[20]:

$$E_g(Al_xGa_{(1-x)}N) = xE_g(AlN) + (1-x)E_g(GaN) - bx(1-x), \quad (1)$$

where the bandgaps of (AlN) and (GaN) at 300 K are 6.25 eV and 3.42 eV, respectively. x represents the aluminum composition, and b is the bowing coefficient, which is set to 0.7 in this study.

3 Results and Discussion

Fig. 2(a) shows the radiative recombination rate of the samples A−C for comparison firstly at a current density of 100 mA/cm^2. It can be clearly seen that the radiative recombination rate of samples B−C is significantly higher than that of sample A. After integrating the three samples, the sample A is only about 2.3 (E17 $cm^{-2}\cdot s^{-1}$), however, sample B is 10.3 (E17 $cm^{-2}\cdot s^{-1}$) and sample C is 10.6 (E17 $cm^{-2}\cdot s^{-1}$). The recombination rate of the sample B−C is severally about 4.47 and 4.61 times of sample A. Fig. 2(b) displays the *I-V* curves for samples A−C.

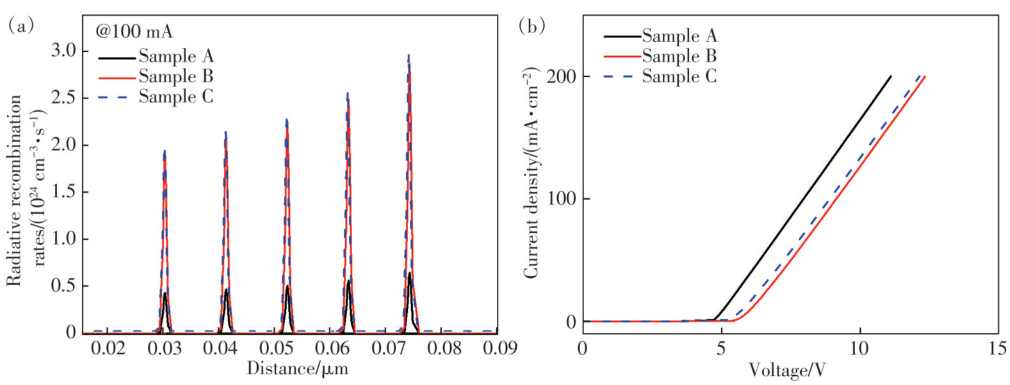

Fig.2 The radiative recombination rates(a) in the multiple quantum wells for samples A−C under current density of 100 mA/cm^2 and the *I-V* curves(b) of samples A−C

The operating voltages of samples B and C are slightly elevated compared to sample A, presumably due to the introduction of quantum barriers, which introduce novel bandgap barriers. Furthermore, as elaborated in the subsequent text, sample C has effectively improved the transportation of charge carriers, leading to a reduction in partial pressure. Consequently, the operating voltage of sample C is lower than that of sample B.

To find out the reasons for the improved performance of samples B and C, we investigate the band samples. In Fig. 3, the band samples at a current density of 100 mA/cm^2 are shown, and the effective barrier heights of the three samples are calculated. From the perspective of the electronic effective barrier of EBL, the values of sample A are only 225. 9 meV and 609. 5 meV, respectively. However, for sample B, the values are 587 meV and 672. 92 meV. For sample C, the values are 609. 8 meV and 694. 82 meV. The effective electronic potential barriers of samples B and C are higher than those of sample A, which prevents electrons from leaking into the P region to a certain extent. And from the perspective of the effective hole potential barrier of EBL, the height of effective hole barrier in sample A is 498. 8 meV, while the height in sample B is 461. 6 meV and the one in sample C is 459. 7 meV. It can be clearly seen that the effective hole barrier height of samples B–C is relatively low, making it easier for holes to enter the active region from the P region. In the active region, the electron concentration is usually greater than the hole concentration. Therefore, as the hole concentration in the active region increases, these increased holes will recombine with the electrons in the active region, thereby improving the radiation recombination rate. Specifically, the difference between the electron concentration and hole concentration in the active region significantly affects the radiation recombination rate. For the reasons mentioned above, it can be inferred that the reason for the increase in radiation recombination rate of samples B–C is the increase in hole concentration in the active region and the constraint on electron leakage in the P region.

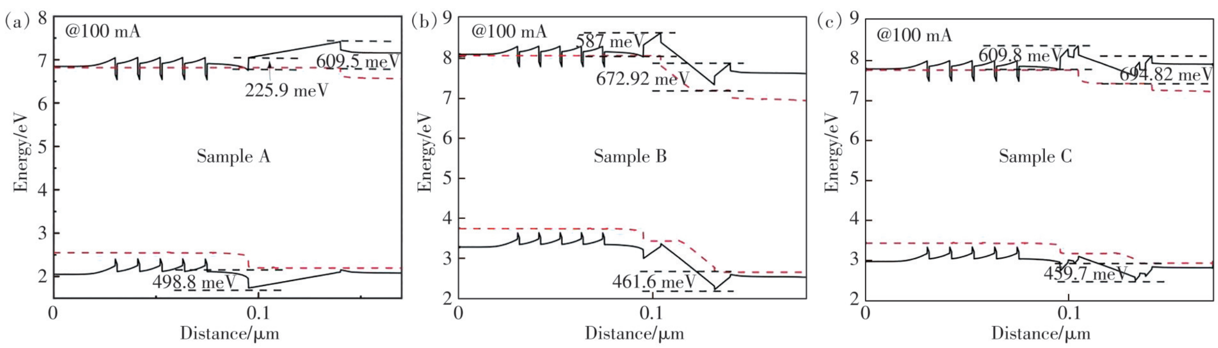

Fig.3　Energy band diagrams of sample A(a), sample B(b), sample C(c)

We further compare the electron concentration and the hole concentration in the active region as shown in Fig. 4. It is clear that the electron concentration of the P region in sample B–C is lower than that in sample A in Fig. 4(a). The hole concentration in the QWs region in Fig. 4(b) can also be obtained, and the hole concentration in samples B–C is higher than that in sample A. This observation is consistent with previous speculation that the improved radiative recombination rate of samples B–C is due to increased hole concentration in the active region and the constraint on electron leakage in the P region.

The increase in hole concentration in the active region can be explained by the EBL interlayer in Fig. 5. Due to the opposite polarization-induced sheet charges ($-\sigma$ and $+\sigma$) on the sides of the EBL depression, there is a polarization field along the $[000\bar{1}]$ direction, and when holes pass through the EBL interlayer, they are subjected to an accelerating electric field. This electric field allows holes to obtain greater energy, thereby reducing the difficulty of holes injection into the active region.

Due to the acceleration effect of this sample on both holes and electrons, so when the acceleration electric field is too large, electron leakage will be more pronounced. Especially when the interlayer of

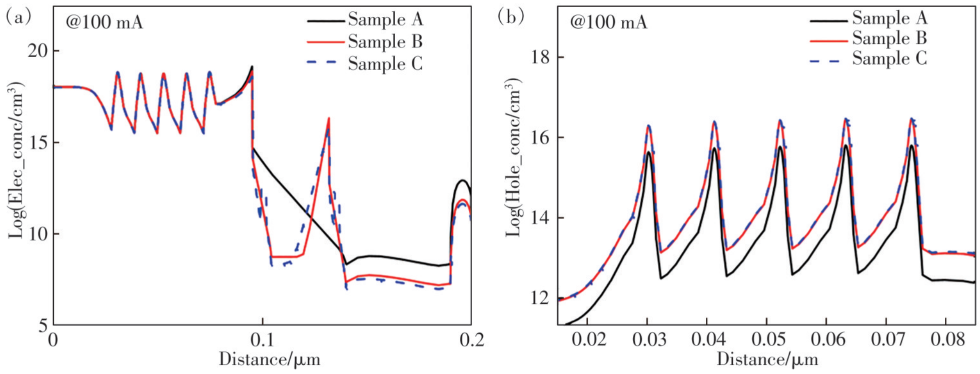

Fig.4 Electron concentration(a) and hole concentration(b) in the active region of samples A-C

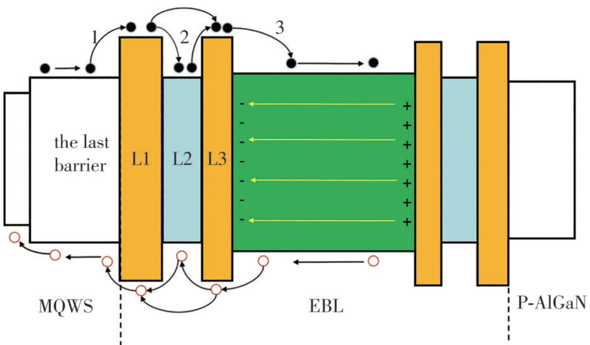

Fig.5 Schematic representation of the electric field and carrier flow within the intermediate layer of the EBL region

the accelerating electric field increases to a certain extent, the electron concentration in the P region significantly increases. Although electron phonon scattering consumes some of the energy of electrons, but some electrons still burst out of the active region.

Therefore, in order to solve the problem of electronic leakage, we further optimize the sample to achieve balanced injection of electrons and holes, such as sample C. As mentioned in Fig. 3, the effective potential barrier for electrons in the EBL of sample C is higher than that of sample B. Additionally, the electron concentration in the P region of sample C is also lower than that of sample B as shown in Fig. 4(a). These further indicate that the EBL with a multi-quantum barrier sample in sample C can enhance its capability to block electron leakage.

We also elaborate on the electron blocking effect based on the aforementioned physical model. As can be observed from Fig. 5, in most cases, the transport of electrons is from path 1 to 2, and then to 3 due to the presence of L2 layer. Since the thickness of L1 layer is relatively thick in sample C, the possibility of the electron tunneling through L1 layer is very low. The electron path of 1-2-3 necessitates two transitions and consumes more energy. So the sample with the multi-quantum barriers, to some extent, prevents electronic leakage. Furthermore, the thickness of the EBL must be meticulously evaluated. Excessive thickness can lead to challenges in light emission, while insufficient thickness may hinder the establishment of a stronger negative electric field. As a result, numerous calculations are necessary to pinpoint the ideal thickness that optimizes performance. It must be pointed out that from the distribution of electric fields in the interlayer area, there is no negative electric field in the EBL region of sample A. However, it can be observed that a large negative electric field in the $[000\bar{1}]$ direction is formed in the depression area of samples B-C, which can provide energy for the holes. As shown in Fig. 6, the energy of the sample B obtained by the hole here is:

$$E = q\int \Phi \cdot \mathrm{d}l, \qquad (2)$$

among them, E is the energy, q is the charge of the hole, $\int \Phi \cdot \mathrm{d}l$ represents the integral of potential difference, representing the potential difference along the path (l)(Φ), and path(l) represents the negative electric field component of the EBL region. The integrated E within the EBL region of sample B is approximately −1.056 9 eV. However, the E of sample C is −0.715 6 eV. After the holes gain energy in this accelerating electric field, it will be easier to reach the active region.

Overall, the negative electric field integral of sample C in the EBL is lower than that of sample B,

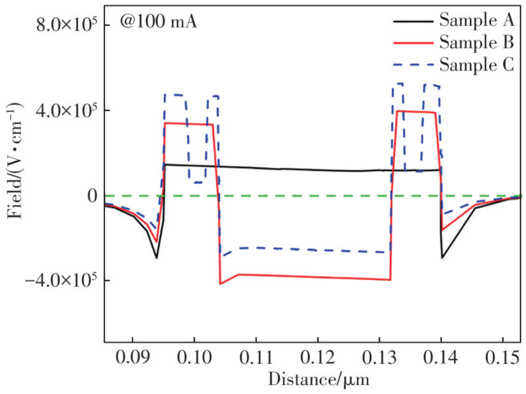

Fig.6　Electric field map of samples A−C in the EBL region

but its radiative recombination rate is higher, possibly because it has a stronger control over electrons. In addition, the novel structure also alleviates partly the negative effect of the polarization. That can be reflected from the electric field near the last layer quantum barrier. As shown in Fig. 6, the electric field bending degree of sample C in this place is significantly lower than that of samples A and B, which indicates that the electric field bending caused by electron stacking in sample C is alleviated to a certain extent. Additionally, in Fig. 2(b), the insertion of structures such as quantum barriers within the EBL of samples B and C introduces additional bandgap barriers, thereby elevating their operating voltages. Nevertheless, sample C exhibits superior carrier transportation characteristics and reduces the partial pressure, ultimately resulting in a lower operating voltage than sample B. In the future, we aim to further optimize the EBL structure, aiming to boost carrier injection rates while simultaneously minimizing operating voltage.

4　Conclusion

In this work, separated multiple quantum barrier EBL has been investigated to improve the performance of AlGaN-based DUV-LEDs with the wavelength shorter than 250 nm. It is confirmed that the DUV-LEDs with separated multi-quantum barriers EBL gives rise to a much higher hole concentration and radiative recombination rate than the conventional EBL configuration. Due to the formation of a hole acceleration zone by the separated interlayer in the EBL and simultaneously raises the effective electron barrier, the hole injection efficiency is significantly increased and multi-quantum barrier sample reduces the electron leakage, thus significantly improving the device performance.

Response Letter is available for this paper at: http://cjl. lightpublishing. cn/thesisDetails#10. 37188/CJL. 20240045.

References:

[1] CHEN Y X, BEN J W, XU F J, *et al.* Review on the progress of AlGaN-based ultraviolet light-emitting diodes [J]. *Fundam. Res.*, 2021, 1(6): 717-734.

[2] YAO Y F, ZOLLNER C J, WANG M, *et al.* Polarization-enhanced p-AlGaN superlattice optimization for GUV LED [J]. *IEEE J. Quant. Electron.*, 2022, 58(4): 3300409.

[3] KHAN A, BALAKRISHNAN K, KATONA T. Ultraviolet light-emitting diodes based on group three nitrides [J]. *Nat. Photon.*, 2008, 2(2): 77-84.

[4] HRAYAMA H, MAEDA N, FUJIKAWA S, *et al.* Recent progress and future prospects of AlGaN-based high-efficiency deep-ultraviolet light-emitting diodes [J]. *Jpn. J. Appl. Phys.*, 2014, 53(10): 100209.

[5] MELLQVIST J, ROSÉN A. DOAS for flue gas monitoring—II. Deviations from the Beer-Lambert law for the U. V. /visible absorption spectra of NO, NO_2, SO_2 and NH_3 [J]. *J. Quantitat. Spectrosc. Radiat. Transfer*, 1996, 56(2): 209-224.

[6] YAMAN M, BAKIRDERE S. Identification of chemical forms of lead, cadmium and nickel in sewage sludge of waste water treatment facilities [J]. *Microchim. Acta*, 2003, 141(1-2): 47-54.

[7] JI X L, YAN J C, GUO Y N, *et al.* Tailoring of energy band in electron-blocking structure enhancing the efficiency of AlGaN-based deep ultraviolet light-emitting diodes [J]. *IEEE Photon. J.*, 2016, 8(3): 1600607.

[8] LU L, DING G G, ZHANG Y, *et al.* Improved performance of AlGaN-based deep ultraviolet light-emitting diode using modulated-taper design for p-AlGaN layer [J]. *Semicond. Sci. Technol.*, 2018, 33(3): 035008.

[9] SIMON J, PROTASENKO V, LIAN C X, *et al*. Polarization-induced hole doping in wide-band-gap uniaxial semiconductor heterostructures [J]. *Science*, 2010, 327(5961): 60-64.

[10] TAO H C, XU S R, ZHANG J C, *et al*. Numerical investigation on the enhanced performance of N-polar AlGaN-based ultraviolet light-emitting diodes with superlattice p-type doping [J]. *IEEE Trans. Electron Dev.*, 2019, 66(1): 478-484.

[11] LANG J, XU F J, GE W K, *et al*. Greatly enhanced performance of AlGaN-based deep ultraviolet light emitting diodes by introducing a polarization modulated electron blocking layer [J]. *Opt. Express*, 2019, 27(20): A1458-A1466.

[12] LU L, WAN Z, XU F J, *et al*. Performance improvement of AlGaN-based deep-ultraviolet light-emitting diodes *via* Si-doping design of quantum barriers [J]. *Superlatt. Microstruct.*, 2017, 109: 687-692.

[13] MOHAMED H, SENGOUGA N, MEFTAH A. Enhancing GaN/AlGaN MQW micro LED optical and electrical performance with a non-uniform LQB [J]. *Trans. Electr. Electron. Mater.*, 2023, 24(5): 469-478.

[14] LIU Z Y, LU Y, WANG Y, *et al*. Polarization modulation at last quantum barrier for high efficiency AlGaN-based UV LED [J]. *IEEE Photon. J.*, 2022, 14(1): 8210208.

[15] DAS S, LENKA T R, TALUKDAR F A, *et al*. High-performance DUV AlGaN multi-quantum well LED with step-graded n-type AlInGaN electron blocking layer [J]. *J. Optoelectron. Adv. Mater.*, 2023, 25(7-8): 311-320.

[16] Crosslight Software Inc. Crosslight APSYS software [EB/OL]. (2020-03-10). http://crosslight.com/products/apsys/.

[17] ZHANG Z H, LIU W, JU Z G, *et al*. Polarization self-screening in [0001] oriented InGaN/GaN light-emitting diodes for improving the electron injection efficiency [J]. *Appl. Phys. Lett.*, 2014, 104(25): 251108.

[18] FIORENTINI V, BERNARDINI F, AMBACHER O. Evidence for nonlinear macroscopic polarization in III-V nitride alloy heterostructures [J]. *Appl. Phys. Lett.*, 2002, 80(7): 1204-1206.

[19] GUO W W, XU F J, SUN Y H, *et al*. Performance improvement of AlGaN-based deep-ultraviolet light-emitting diodes by inserting single spike barriers [J]. *Superlatt. Microstruct.*, 2016, 100: 941-946.

[20] VURGAFTMAN I, MEYER J R, RAM-MOHAN L R. Band parameters for III-V compound semiconductors and their alloys [J]. *J. Appl. Phys.*, 2001, 89(11): 5815-5875.

申国文(1997-),男,安徽芜湖人,硕士研究生,2021年于安徽工程大学获得学士学位,主要从事光电子材料及其器件的研究。

E-mail: 1877610696@qq.com

鲁麟(1980-),男,安徽芜湖人,博士,教授,硕士生导师,2009年于北京大学获得博士学位,主要从事Ⅲ-Ⅴ族宽禁带半导体光电子材料及器件的研究。

E-mail: llu-wh@qq.com